

# The ultrafast East Pacific Rise: instability of the plate boundary and implications for accretionary processes

BY MARIE-HELÈNE CORMIER

*Lamont-Doherty Earth Observatory, Columbia University, NY 10964-8000, USA*

The Pacific–Nazca plate boundary evolves continuously through the frequent, rapid propagation of ridge segments and through the growth or abandonment of microplates. Propagation events can initiate at overlapping spreading centres only a few kilometres wide as well as within large transform faults. This instability of the ultrafast East Pacific Rise (EPR) probably results from the presence of a hot, thin lithosphere in the axial region, coupled with a melt supply that may be temporally or spatially variable. It indicates that along-axis magma transport can be efficient at rates corresponding to propagation rates, up to  $1000 \text{ mm yr}^{-1}$ . To a first-order, the tectonic segmentation of the ridge correlates with along-axis variations of the axial morphology and other physical parameters suggesting a diminished magmatic budget near offsets larger than a few kilometres. A similar correlation between axial segmentation and variations in physical characteristics at the Mid-Atlantic Ridge (MAR) is commonly interpreted to indicate that mantle upwelling is focused near mid-segment at slow-spreading ridges (three dimensional). Accordingly, mantle upwelling may be focused at discrete intervals along the ultrafast EPR. However, fluctuations of the along-axis characteristics are considerably more subdued at the EPR than at the MAR. This has been interpreted to reflect smoothing of the structural variations by efficient transport within the shallow crust and upper mantle of the material brought up through focused upwelling. Alternatively, it has been argued that mantle flow is essentially uniform along-axis (two dimensional) at the faster spreading centres. It is proposed here that the actual pattern of mantle flow along the EPR combines aspects of both models. Fast spreading centres may be supplied by vertical mantle flow nearly continuously along-axis, but the intensity of this upwelling can fluctuate both temporally and spatially, hence favouring along-axis transport away from the magmatically most robust areas.

---

## 1. Introduction

The Pacific–Nazca plate boundary spreads apart at  $125\text{--}152 \text{ mm yr}^{-1}$ , the fastest rate of the entire mid-ocean ridge system (DeMets *et al.* 1994). Over the approximately 4000 km spanned by this plate boundary, the morphology of the axial region varies remarkably little (Macdonald *et al.* 1988*a*; Lonsdale 1989; Sinton *et al.* 1991). It is defined by a linear high, 5–15 km wide and rising 300–500 m above the surrounding seafloor. This axial high continues uninterrupted for distances of

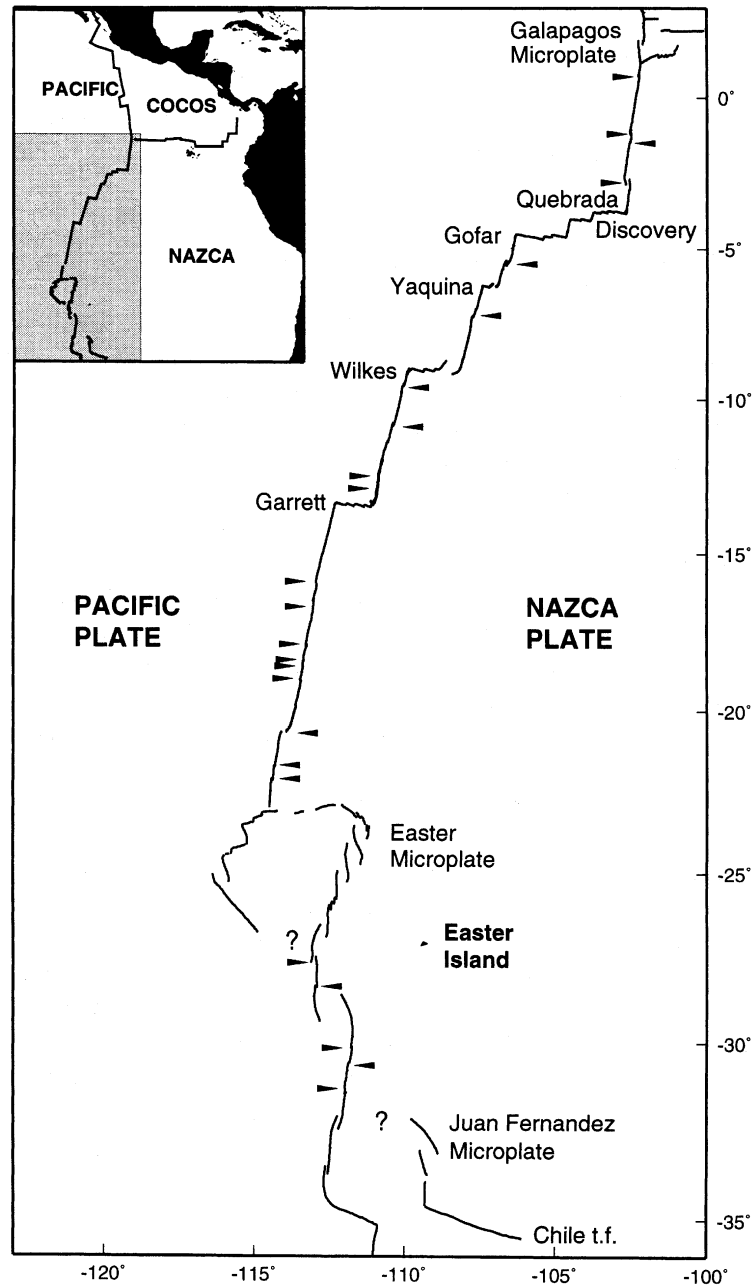


Figure 1. Map view of the southern EPR. Inset shows location relative to South America. The plate boundaries are compiled from Tighe *et al.* (1988), Macdonald *et al.* (1988b), Lonsdale (1989), Naar & Hey (1991), Larson *et al.* (1992) and Hey *et al.* (1995). Arrow heads indicate the location of OSCs with offset greater than 3 km (microplates excluded). Arrows point to the west for right-stepping OSCs, and to the east for left-stepping OSCs.

25–250 km (figure 1). Except in the vicinity of Easter hot spot or along short intratransform spreading centres, axial depths undulate gently between 2500–3000 m (figure 2). Direct observations from submersible and towed-camera surveys indicate

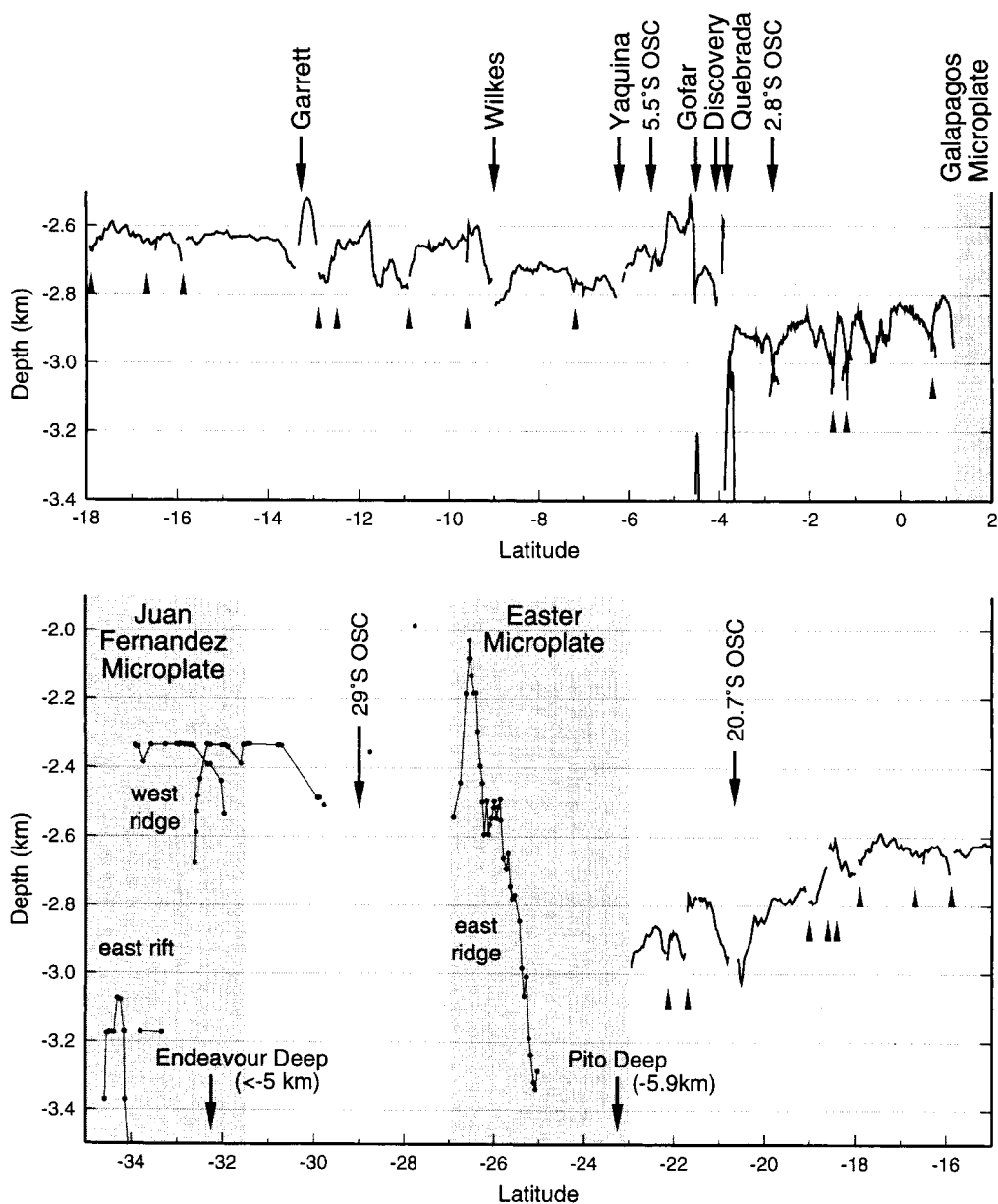


Figure 2. Zero-age depth variations as a function of latitude. North of 23° S, depths are compiled from continuous SeaBeam swath bathymetry data (Macdonald *et al.* 1988; Lonsdale 1989; Scheirer *et al.* 1993). South of 23° S, published bathymetry data are incomplete, and axial depths are derived from discrete Sea Beam crossings of the ridge axis (Naar & Hey 1986; Francheteau *et al.* 1987). Small arrow heads indicate discontinuities with 3–8 km offset. Axial depths near discontinuities are not systematically displayed; they typically increase by a 100–300 m at large OSCs, and vary by 100–1500 m at intratransform spreading centres (Lonsdale 1989; Fox & Gallo 1989).

that the narrow axial summit (0.2–4 km wide) is the locus of the most recent volcanism (Macdonald *et al.* 1982; Francheteau & Ballard 1983; Renard *et al.* 1985; Morton & Ballard 1986; Bicknell *et al.* 1987; Holler *et al.* 1990; Macdonald *et al.*

1988*b*; Urabe *et al.* 1995; Auzende *et al.* 1996). A zone of crustal accretion at most 1–2 km wide is also indicated by the narrowness of the axial magma chamber (less than 1 km) detected by seismic methods (Kent *et al.* 1994), the sharpness of the magnetic reversal boundaries on the rise flanks (Sempéré *et al.* 1987), and the rapid transition from extrusives to sheeted dikes in the upper crust (Hooft *et al.* 1996).

This uniformity and orderliness of the axial morphology at the ultrafast EPR is similar to that of other sections of the EPR spreading at slightly slower rates (80–125 mm yr<sup>-1</sup>), along the Pacific–Cocos plate boundary to the north (Macdonald *et al.* 1984; Macdonald *et al.* 1992) and along 2400 km of the Pacific–Antarctic plate boundary to the south (Lonsdale 1994). It contrasts with the dramatic variations in morphology of the rift valley along slow spreading ridges. At the Mid-Atlantic Ridge, seismic, gravity and geological studies reveal that the systematic 500–2000 m deepening of the rift valley toward the extremities of ridge segments correlates with the accretion of a progressively thinner crust (White *et al.* 1984; Lin *et al.* 1990; Tolstoy *et al.* 1993; Detrick *et al.* 1995; Cannat *et al.* 1995). These crustal thickness variations reach a few kilometres in amplitude, and are thought to reflect the three-dimensional geometry of mantle and magma circulation that feed slowly spreading ridge segments. In comparison, the subdued morphological variations along the fast spreading EPR suggest that magma supply is relatively steady-state and uniform. Nonetheless, although subdued, these morphological variations correlate with the tectonic segmentation of the EPR. This systematic correlation has been used to argue that, on the contrary, mantle upwelling is focused at intervals along the ridge, and that melt is subsequently transported along-strike within the crust or upper mantle. This paper reviews the arguments for and against uniform accretionary processes at the EPR. In particular, the detailed kinematic evolution of the southern EPR reveals that axial segmentation is unstable at time scales as small as 0.1 Ma, and that ridge segment propagation across ridge offsets of any size is frequent. This suggests that along-strike magma transport of material can be efficient at rates at least as high as propagation rates, up to *ca.* 1000 mm yr<sup>-1</sup>.

## 2. The present plate boundary

At intermediate and fast spreading centres, 2–30 km ridge offsets are accommodated by overlapping spreading centres (OSCs) rather than by the classic ridge-transform-ridge geometry (Macdonald *et al.* 1988*a*). Along the ultrafast EPR, OSCs are irregularly spaced at intervals of 25–300 km (Macdonald *et al.* 1988; Lonsdale 1989; Sinton *et al.* 1991; Scheirer *et al.* 1996*a*). They generally have offset smaller than 8 km, and their presence does not significantly affect the regional linearity of the plate boundary (figure 1). North of the Easter microplate, only three OSCs have offsets larger than 10 km: the 2° 45' S OSC (27 km offset), the 5° 30' S OSC (15 km offset), and the 20° 40' S OSC (15–20 km offset) (Rea 1981; Lonsdale 1983; Macdonald *et al.* 1988*b*). Offsets larger than 30 km are clustered along two sections of the EPR. From 3° 50' S to 13° S, six right-stepping transform faults gradually offset the EPR by about 750 km (Searle 1983; Fox & Gallo 1989; Lonsdale 1989). These are the only transform faults along the ultrafast EPR. Each one is a 'multiple' transform fault, consisting of a few parallel transform strands linked by short (less than 15 km) intratransform spreading centres. South of 23° S, where full spreading rates peak at 147–152 mm yr<sup>-1</sup>, the plate boundary displays a more complex geometry. It is straddled by two microplates a few hundred kilometres across, the Easter microplate and

the Juan Fernandez microplate (Searle *et al.* 1989; Larson *et al.* 1992). Between these two microplates, the EPR is offset by a 120 km wide OSC, the largest non-transform offset mapped along the mid-ocean ridge system (Hey *et al.* 1995). Each of these three features imparts a left-stepping jog to the ridge axis, and together they correspond to a cumulative offset of *ca.* 350 km. From 23–35° S, the full spreading rate is accommodated at one simple ridge segment only along the 30–32° S section. Outside of this latitudinal range, crustal accretion is partitioned between two spreading centres, either between the east and west ridges of the Easter and Juan Fernandez microplates, or between the overlapping ridges of the large 29° S OSC.

### 3. Kinematic evolution of the southern EPR since 7 Ma

Recent swath surveys of the southern EPR which extend off-axis on to seafloor at least 1 my old reveal that although the axis of accretion is narrowly defined everywhere, it can rapidly shift location. On a time scale of a few hundred thousand years, some ridge segments propagated hundreds of kilometres, while entire sections of ridge became abandoned. These propagation events initiated at discontinuities ranging from OSCs only a few kilometres wide to transforms with a few hundred kilometre offsets. This section and table 1 summarize those events that have been recognized, following the ultrafast EPR from south to north.

Magnetic and swath sonar data indicate that both the Juan Fernandez and Easter microplates evolved from propagating ridges at offsets of the EPR. The ridges which bound these two microplates to the east propagated northward, and progressively overlapped a few hundred km of the EPR (Francheteau *et al.* 1987; Searle *et al.* 1989; Naar & Hey 1991; Larson *et al.* 1992; Rusby & Searle 1995). Recent, extensive side scan surveys indicate that both east ridges originated at about 6 Ma from within transform faults rather than at OSCs (figure 3*d*; Bird & Naar 1994). The east ridge of the Juan Fernandez microplate propagated from within the Chile transform, and the east ridge of the Easter microplate propagated from within the now abandoned SOEST fracture zone, the fossil trace of which is located about 60 km south of Easter Island (Hey *et al.* 1995). Crust initially formed at both east ridges is truncated by these fracture zones, indicating that propagation did not originate at a classic ridge-transform intersection. Rather, intratransform spreading centres must have served as the focal points for these propagation events (Bird & Naar 1994).

The large left-stepping 29° S OSC located between these two microplates has been migrating southward at *ca.* 120 mm yr<sup>-1</sup> (figure 3*c*; Hey *et al.* 1995). In the course of this migration, the overlap region is regularly rafted onto the Nazca plate; therefore, despite its large width (120 km), the overlap region does not define a rigidly rotating microplate. A detailed kinematic analysis shows that propagation originated at the SOEST transform fault (Korenaga & Hey 1996). The SOEST offset evolved from a classic transform fault to an OSC configuration at *ca.* 1.95 Ma, and initiated its rapid southward migration at *ca.* 1.5 Ma (figure 3*c*). The propagating ridge segment is roughly aligned with the east rift of the Easter microplate, which propagates in the opposite direction. Both propagation events are directed away from the Easter hot spot.

The right-stepping OSC at 20° 40' S is a 'duelling propagator', the overlapping ridge tips of which have alternatively propagated and retreated over distances greater than 50 km (Macdonald *et al.* 1988*b*; Perram *et al.* 1993). The net migration rate since 2 Ma is only *ca.* 20 mm yr<sup>-1</sup>, southward. Based on sparser magnetic coverage

Table 1. Summary of off-axis swath sonar surveys and their kinematic interpretations

latitudes	geometry of plate boundary	swath sonar data collected off-axis	kinematic interpretation	references
1° 10' N–3° S Galapagos triple junction	Galapagos microplate	Some GLORIA and SeaBeam coverage	Microplate initiated at <i>ca.</i> 1 Ma	Searle & Francheteau (1986) Lonsdale (1988)
3–5° S Quebrada, Discovery and Gofar transform faults	Right-stepping multiple transform faults	GLORIA side-scan coverage, out to 1–2 Ma	<i>ca.</i> 1 Ma old Nazca seafloor appears rotated, which is suggestive of large scale propagation event: present transforms' geometry is less than 2 Ma old	Searle (1983, 1984) Lonsdale (1989)
7–9° 30' S Wilkes transform fault and 'nanoplate'	Right-stepping multiple transform fault and nanoplate	Hydrosweep out to <i>ca.</i> 1.6 Ma	Propagation of northern segment into transform domain since 3 Ma, and formation of nanoplate	Cochran <i>et al.</i> (1993) Goff <i>et al.</i> (1993)
15° 30–19° S MELT experiment area	Staircases of left-stepping OSCs	SeaMARC II, HMR-1 and Sea Beam 2000, out to 6 Ma	Several propagation events at rates greater than 1000 mm yr <sup>-1</sup> . Propagating segments often initiated within OSCs, bisecting them into smaller OSCs	Cormier & Macdonald (1994) Cormier <i>et al.</i> (1996) Scheirer <i>et al.</i> (1996a)

Table 1. *Cont.*

latitudes	geometry of plate boundary	swath sonar data collected off-axis	kinematic interpretation	references
20–21° S dueling propagator	Right-stepping 20° 40' S OSC (15–20 km offset)	SeaBeam and SeaMARC II, out to 2 Ma	OSC alternatively migrates northward and southward, with an overall 20 mm yr <sup>-1</sup> southward migration rate	Macdonald <i>et al.</i> (1988b) Perram <i>et al.</i> (1993)
23–27° S Easter microplate	Microplate <i>ca.</i> 450 km across	GLORIA coverage of entire microplate; some Sea Beam and SeaMARC II coverage	Northward propagation of east rift initiated at <i>ca.</i> 6 Ma within SOEST transform	Francheteau <i>et al.</i> (1988) Naar & Hey (1991) Searle (1989) Rusby & Searle (1995)
27–32° S	Left-stepping 29° S OSC (120 km offset)	GLORI-B and SeaBeam 2000 out to 2.5 Ma	Ridge axis propagated south across SOEST transform at 1.9 Ma, and formed large OSC. Since then, OSC has net southward migration rate of 120 mm yr <sup>-1</sup>	Klaus <i>et al.</i> (1991) Hey <i>et al.</i> (1995) Korenaga & Hey (1996)
31–35° S Juan Fernandez microplate	Microplate <i>ca.</i> 350 km across, at triple junction	GLORIA coverage of entire microplate; some SeaBeam and Hydrosweep coverage	Northward propagation of east rift initiated at <i>ca.</i> 6 Ma within Chile transform	Francheteau <i>et al.</i> (1987) Larson <i>et al.</i> (1992) Bird & Naar (1994) Bird <i>et al.</i> (1996)

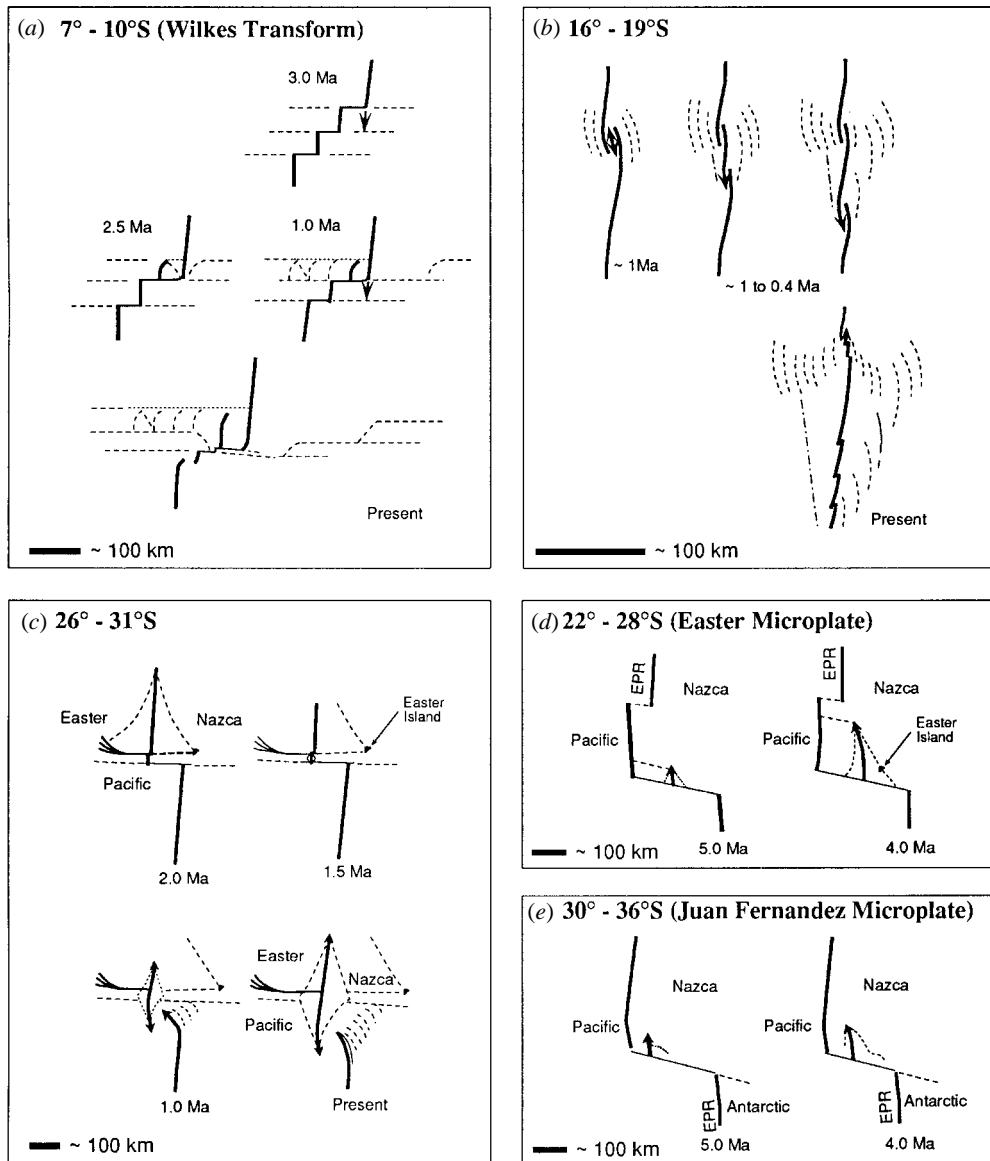


Figure 3. Schematic time frames illustrating the recent kinematic evolution of several sections of the ultrafast EPR. Thick lines indicate actively spreading EPR, and dash lines abandoned ridges or fracture zone traces. Approximate scale bars are indicated for each area. (a) Evolution of Wilkes transform domain, after Goff *et al.* (1993). (b) Evolution of EPR at 16–19° S, after Cormier *et al.* (1996). (c) Evolution of 29° S propagator, after Hey *et al.* (1995). (d) and (e) Origin of Easter and Juan Fernandez microplates, after Bird & Naar (1994).

beyond seafloor 2 Ma old, this slow overall migration rate appears to have been sustained since at least 6 Ma (D. S. Wilson, personal communication).

Although only small offset (less than 8 km) left-stepping OSCs presently dot the EPR between 15 and 19° S, combined analysis of side-scan and magnetic data shows that up to 1 Ma this section of the ridge was marked instead by a few left-stepping OSCs with 15–20 km offsets (figure 3b; Cormier & Macdonald 1994; Cormier *et al.*

1996). These OSCs were bisected into smaller OSCs by new spreading segments forming within their overlap basins. The smaller OSCs proceeded to migrate rapidly (greater than  $500 \text{ mm yr}^{-1}$ ) and were further bisected by newly spawned ridge segments until the present staircase of small, left-stepping OSCs was achieved.

The Wilkes transform geometry has been continuously evolving since at least 3 Ma, as revealed by a large scale Hydrosweep survey (figure 3a; Goff *et al.* 1993). Stepwise southward propagation of the EPR into the Wilkes transform domain initiated at *ca.* 3 Ma, as indicated by the successive abandonment of two transform strands. Secondary rifting west of the EPR has formed a 'nanoplate' about 50–60 km across which is rotating counterclockwise and may eventually evolve into a microplate.

GLORIA side scan images collected between 3 and 5° S over the Quebrada, Gofar and Discovery transforms system show that the seafloor fabric of *ca.* 1 Ma old Nazca crust is rotated counterclockwise with respect to the ambient orientation (Searle 1983). Accordingly, poorly resolved magnetic lineations suggest that the spreading system north of Yaquina Transform had an overall strike highly oblique to Pacific–Nazca relative motion as recently as 0.7 Ma (Lonsdale 1983). Hence, the EPR between 3 and 7° S probably reached its present configuration since 1 Ma.

The origin of all six transform faults between 3 and 13° S may be related to the creation and abandonment of Bauer paleo-microplate (Lonsdale 1989). Large scale northward propagation of the EPR beyond the right-stepping Bauer transform between 10 and 7 Ma created the Bauer microplate. Spreading ceased on the east ridge of the microplate at about 6–5 Ma, and a staircase of new transforms developed on the remaining west ridge as the relative motion rotated counterclockwise from Pacific–Bauer to Pacific–Nazca (Lonsdale 1989). Although not imaged with swath sonar system, the boundaries of the Bauer paleo-microplate on the Nazca plate are plainly visible on recent maps of free-air anomaly derived from satellite altimetry data (Sandwell *et al.* 1994). These boundaries delimit an area about 1100 km across, three to four times wider than Easter or Juan Fernandez microplates.

Hence, based on detailed kinematic evolution of some of its sections, the ultrafast EPR appears to be unstable at time scale of 1 Ma or less. Rapid ridge propagation is common, and occurs at axial discontinuities with offsets ranging anywhere from a few kilometres to a few hundred kilometres. In several instances, propagation apparently initiated at short spreading segments located within axial discontinuities. Averaged over several 100 000 yr, propagation rates range from 10–20  $\text{mm yr}^{-1}$  (near-stationary) to greater than 500  $\text{mm yr}^{-1}$  (ultra rapid).

#### 4. Instability of the tectonic segmentation

Although large scale propagation events are also recognized at slow and intermediate spreading centres (Phipps Morgan & Sandwell 1994; Gente *et al.* 1995; Auzende *et al.* 1995), the stability of first order segmentation apparently decreases with increasing spreading rates. This is indicated primarily by the fact that off-axis traces of transform and non-transform discontinuities at slow spreading rates remain subparallel to the spreading direction for many million years, and give the seafloor a distinct 'crenulated' texture (Phipps Morgan & Parmentier 1995). Ridge propagation along the Mid-Atlantic Ridge has not succeeded in disrupting the overall plate boundary geometry inherited from the initial continental break-up, even though the spreading direction has at times rotated by *ca.* 30° (Tucholke & Schouten 1989). In contrast, the paucity of transform faults along the ultrafast EPR may reflect the tendency

for ridge segments to episodically propagate across transform domains (Naar & Hey 1989a). In this way, transform faults, or sections of transform fault defined by intratransform spreading centres, may evolve into large OSCs (see, for example, the Yaquina transform fault), nanoplates (see, for example, the Wilkes transform fault), or microplates (see, for example, the SOEST and Chile transform faults).

Ridge propagation at faster spreading rates is favoured by the rheology of the lithosphere. For equivalent spatial offsets of the ridge axis, the lithosphere abutting the ridge tips is about an order of magnitude younger (thinner) at the EPR than at the MAR. A thinner lithosphere will decrease the viscous resistant forces to propagation and thus promote propagation of a ridge tip (Phipps Morgan & Parmentier 1995). However, no general model has yet emerged which can consistently predict the direction of propagation. Each proposed model can account for some regional propagation patterns, but fails to satisfactorily predict other propagation patterns, suggesting that a diversity of factors must govern propagation, or that the principal control on propagation has yet to be understood.

Changes in spreading direction are often associated with large scale propagation events (Wilson *et al.* 1984; Atwater *et al.* 1989). A proposed clockwise change in the Pacific–Nazca relative motion of a few to several degrees in the past several my could explain why all the right-stepping transforms are multiple, ‘leaky’ transforms (Searle 1983), could account for the existence of a staircase of small left-stepping OSCs between the Garrett transform fault and 20° 40′ S (Lonsdale 1989), and could have initiated the growth of the Easter and Juan Fernandez microplates through the propagation of intratransform spreading centres (Bird & Naar 1994). Indeed, variations in the orientation of fault scarps and abyssal hills with seafloor age indicate that the spreading direction along the southern EPR has rotated clockwise by a few to several degrees since 5–6 Ma (Goff *et al.* 1993; Cormier *et al.* 1996). However, although ridge propagation represents an effective mechanism for adjusting the orientation of the ridge axis to a new spreading-normal direction (Wilson *et al.* 1984), the direction of propagation cannot be predicted from the change in spreading direction. The associated change in the far field stress is expected to affect two offset ridge segments equally rather than favouring one of them (Phipps Morgan & Parmentier 1985).

Hey *et al.* (1980), Phipps Morgan & Parmentier (1985) and Phipps Morgan & Sandwell (1994) suggest that ridge propagation is driven by the excess relief of a ridge segment, such that the most prominent segment will prevail over the adjacent ones. This model applies well to the pattern of propagation at 16–19° S, where all OSCs are migrating away from the shallow magmatically robust 17–18° S area, and to the east rift of the Easter microplate and the 29° S OSC, which are both propagating away from the shallow region surrounding the Easter hot spot. However, this mechanism cannot explain why new propagating segments sometime initiate within or close to OSCs (Cormier *et al.* 1996) and transform faults (Bird & Naar 1994), where the ridge axis was presumably deeper.

Based on fracture mechanics theory, Macdonald *et al.* (1991) propose that the relative lengths of the segments on either side of an OSC may govern its migration direction, so that the longer ridge segment will lengthen at the expense of the shorter one. Although this suggestion applies relatively well to several first- and second-order segments of the EPR, it, again, cannot explain the spawning of propagating segments from within OSCs or transform faults.

Lonsdale (1994) suggests that the migration direction of an OSC is governed by

its offset direction (left- or right-stepping) and the migration direction of the ridge axis relative to the asthenosphere. According to this model, an OSC will migrate in a direction which transfers the lithosphere from the ‘leading flank’ to the ‘trailing flank’ of a laterally migrating spreading centre. Over time, this would lead to systematic spreading asymmetry of the ridge axis. Indeed, the southern EPR is generally spreading faster to the east, while it is slowly migrating westward (Gripp & Gordon 1990). The above model predicts that left-stepping OSCs should migrate south, and right-stepping should migrate north. This prediction is not supported by the slow southward migration of the right-stepping 20° 40′ S OSC since 2 Ma (Macdonald *et al.* 1988*b*; Perram *et al.* 1993), the northward propagations of the east rifts of the Easter and Juan Fernandez microplates (Bird & Naar 1994), or the northward propagation of the left-stepping 16° 55′ S OSC (Cormier *et al.* 1996).

Ridge propagation may also be triggered and sustained by local increase in the melt supplied to the EPR. Between 16 and 19° S, propagation events since 1 Ma have been directed away from 17–17° 30′ S, where the ridge presently is in a robust magmatic stage (Cormier *et al.* 1996). Prior to 1 Ma, a large offset (15–20 km) OSC was located at that latitude, and was, in all likelihood, associated with a relatively starved magmatic supply. Waxing and waning of the melt supply may be cyclical and related to the dynamics of mantle upwelling, as has been suggested for the MAR (Tucholke & Lin 1994; Jha *et al.* 1995; Gente *et al.* 1995). Alternatively, the westward migrating EPR may be approaching a mantle thermal anomaly or an ‘easily melted’ mantle heterogeneity located beneath the Pacific plate, which would be recently diverted toward the ridge axis near 16–19° S. There are several lines of evidence for the presence of such a mantle anomaly. Between Garrett transform fault and Easter microplate, the Pacific plate has an anomalously low subsidence rate, consistent with the presence of a hot thermal anomaly in the mantle beneath it (Rea 1978), or with a lateral temperature gradient in the mantle with temperatures increasing to the west (Cochran 1986). A lateral temperature variation in the mantle could also explain the westward decrease in residual gravity anomalies (Cormier *et al.* 1995; Magde *et al.* 1995). Seamounts are anomalously numerous on the Pacific plate within that region, which may indicate the presence of off-axis mantle heterogeneities (Shen *et al.* 1993, 1995; Scheirer *et al.* 1996). Finally, based on isotopic and trace element characteristics of zero-age basalts, Mahoney *et al.* (1994) have suggested that a discrete mantle heterogeneity may be entering into the axial melt zone between 16 and 19° S, although from which direction is uncertain.

## 5. Structure and rheology of the axial region

Seismic studies along several sections of the EPR have documented the existence of a seismic low velocity zone (LVZ) beneath the ridge crest, which extends from 1–2 km below the seafloor down to the base of the crust and is a few to several kilometres wide (Detrick *et al.* 1993; Harding *et al.* 1989; Vera *et al.* 1990; Toomey *et al.* 1990; Caress *et al.* 1992; Mutter *et al.* 1995). At 9° 30′ N, the largest velocity anomaly is confined to a zone less than 2 km wide and less than 1.5 km thick in the mid crust (Toomey *et al.* 1990). The overall small velocity anomaly (less than 1 km s<sup>-1</sup>) associated with the LVZ precludes the existence of a large melt fraction, and the LVZ is generally interpreted as a mostly solidified plutonic section (Toomey *et al.* 1990; Vera *et al.* 1990; Harding *et al.* 1989). In about 60% of the surveyed sections of the EPR, a seismic reflector is tied to the top of the LVZ which can be

traced nearly continuously for several tens of kilometres along the ridge axis (Detrick *et al.* 1993). The characteristics of this reflector are consistent with those expected from an interface between magma and overlying crustal rocks. Further analysis of this reflector constrains the axial magma chamber (AMC) to be a narrow sill-like body probably less than a few hundred metres thick (Kent *et al.* 1990). Between the Garrett transform fault and 20° S, its width is only 400–1050 m and it is as shallow as 0.7–1.5 km below seafloor (Detrick *et al.* 1993; Kent *et al.* 1994; Mutter *et al.* 1995; Tolstoy *et al.* 1996).

Diverse magma types reflecting distinct mantle source compositions are often sampled at close intervals along the EPR, which constrains chemically coherent magma bodies in the crust to be a few kilometres long only, sometimes less (Langmuir *et al.* 1986; Sinton *et al.* 1991). This length scale is significantly shorter than the distance over which a continuous AMC reflector is observed, and probably indicates that along-strike mixing of melts is inhibited by the small thickness of the reservoir (Macdonald *et al.* 1988a; Sinton & Detrick 1992). Furthermore, based on detailed analysis of the seismic data, Hussenoeder *et al.* (1996) argue that this melt lens is actually partly crystallized, and that in some cases it may contain as much as 60% crystal. High crystal content would also inhibit along-strike mixing within the magma reservoir.

A few models have been proposed for the thermal structure of the EPR which takes into account the seismic results (Wilson *et al.* 1988; Phipps Morgan & Chen 1993; Henstock *et al.* 1993). Although they differ slightly in their details, all three models predict that the crustal volume which underlies the AMC down to the base of the crust is at temperatures close to that of the melt lens, *ca.* 1100–1200 °C. The rheology of gabbros at these high temperatures is not well constrained. The melt fraction is generally inferred to increase up section, but the estimated range varies from 5–10% (Nicolas 1993), to 0–100% (Sinton & Detrick 1992). The rigidus is the temperature below which the magma is a crystal bounded aggregate which behaves rheologically like a solid. Marsh (1989) proposed that the rigidus for MORBs corresponds to 50–60% crystal fraction, implying that the volume underlying the melt lens will behave mostly rigidly. Nicolas *et al.* (1993) suggest on the contrary that the gabbroic crystal mush (90% crystal volume) is close to its rigidus temperature and could dynamically convect. This inference is based on the foliation patterns in ophiolitic gabbros and on laboratory experiment.

It is largely assumed that crustal thicknesses vary little along the EPR, averaging 6–7 km (White *et al.* 1992; Chen 1992). Yet, actual direct crustal thickness measurements are rare. Admittedly, seismic refraction experiments in the eastern Pacific have only occasionally detected  $P_n$  arrivals from the moho. Crustal thicknesses are usually inferred (rather than constrained) from vertical two-way travel times to the moho and from the pattern of precritical mantle reflection arrivals (Harding *et al.* 1989; Vera *et al.* 1989). However, rather than marking a petrologic boundary between crust and mantle, the seismic reflection moho may indicate the top of the crust–mantle transition zone; that is, a boundary between the purely mafic portion of the crust and the region with ultramafic presence (Collins *et al.* 1986; Barth & Mutter 1996). Vertical two-way travel times to the moho are quite variable along portions of the northern EPR, and short-wavelength crustal thickness variations of up to *ca.* 2.6 km has been recently proposed to exist near 9 and 13° N (Barth & Mutter 1996). If the seismic moho marked the top of the crust–mantle transition zone rather than the base of the magmatic crust, these short wavelength variations could also reflect the

variable thickness of the transition zone rather than the total thickness of crust plus transition zone.

## 6. Ridge segmentation and variability of axial characteristics

Ridge segments probably represent the primary units of crustal accretion, and their spacing, morphology and migration along axis provide clues to the architecture of magmatic plumbing that feed the ridge axis. The best surveyed section of the southern EPR stretches from the Garrett transform fault to the Easter microplate, and the following focuses mostly on the variability of the geological and geophysical parameters along that section of the ridge and compares it to its axial segmentation (figure 4).

Zero-age depth variations at wavelengths of a few to several hundred km most likely reflect regional anomalies in the temperature and composition of the mantle (LeDouaran & Francheteau 1980; Klein & Langmuir 1987). Temperature variations in the mantle may account for the greater depths (2800–3000 m) of the equatorial EPR (Bonatti *et al.* 1995) and the shallower depths (2000–2600 m) south of 26° S near the Easter hotspot (Schilling *et al.* 1985) (figure 2). Superimposed over these regional variations, smaller fluctuations in zero-age depths generally correlate to the tectonic segmentation of the ridge axis (Macdonald & Fox 1988; Macdonald *et al.* 1988a). Axial depths tend to plunge by a few to several hundred metres toward OSCs and transform faults, and the magnitude of this deepening increases with the width of the offset (Macdonald *et al.* 1991). However, other factors than proximity to ridge offsets must also control the short wavelength fluctuations in zero-age depths along the superfast EPR. Depth variations may be greater from one segment to the next than along any individual segment. In particular, intratransform spreading centres often stand a few to several hundred metres deeper or shallower than the neighbouring ridge segments (Lonsdale 1989). Some segments also maintain a constant depth ( $\pm 20$  m) almost right up to their extremities. The series of ridge segments between Garrett transform and 18° S have a nearly flat summit, at *ca.* 2630 m. Seemingly minor discontinuities can also represent significant boundaries in axial depth characteristics. Hence, the small 8° 38' S OSC (*ca.* 1.2 km offset) marks a boundary between a 150 km long northern segment which has a constant axial depth (*ca.* 2725 m) and a southern segment that steadily deepens by a few hundred metres toward the Wilkes transform (Cochran *et al.* 1993).

The axial segmentation of the EPR is in fact better correlated to the width of the axial high than to the axial depth. For most segments, the axial high narrows significantly toward segment ends, as indicated by the pinching of bathymetry contours. In particular, even though the zero-age depth is nearly constant between 7° 12'–8° 38' S or 14–18° S, depths measured just 2 km from the ridge axis (along the 0.02–0.03 Ma isochrons) increase by a few 100 m toward segment ends (Cochran *et al.* 1993; Scheirer & Macdonald 1993). This decoupling between the on-axis depth variations and the near-axis depth variations suggest that they are responding to somewhat different processes.

The measure of the cross-sectional area of the ridge axis integrates both axial depth and axial width information, and has proven to be a sensitive indicator of magma supply along the EPR, as confirmed from several other parameters (Scheirer & Macdonald 1993). However, large cross-sectional areas do not correlate with thicker accumulation of extrusives. Although data are few, along- and across-axis seismic

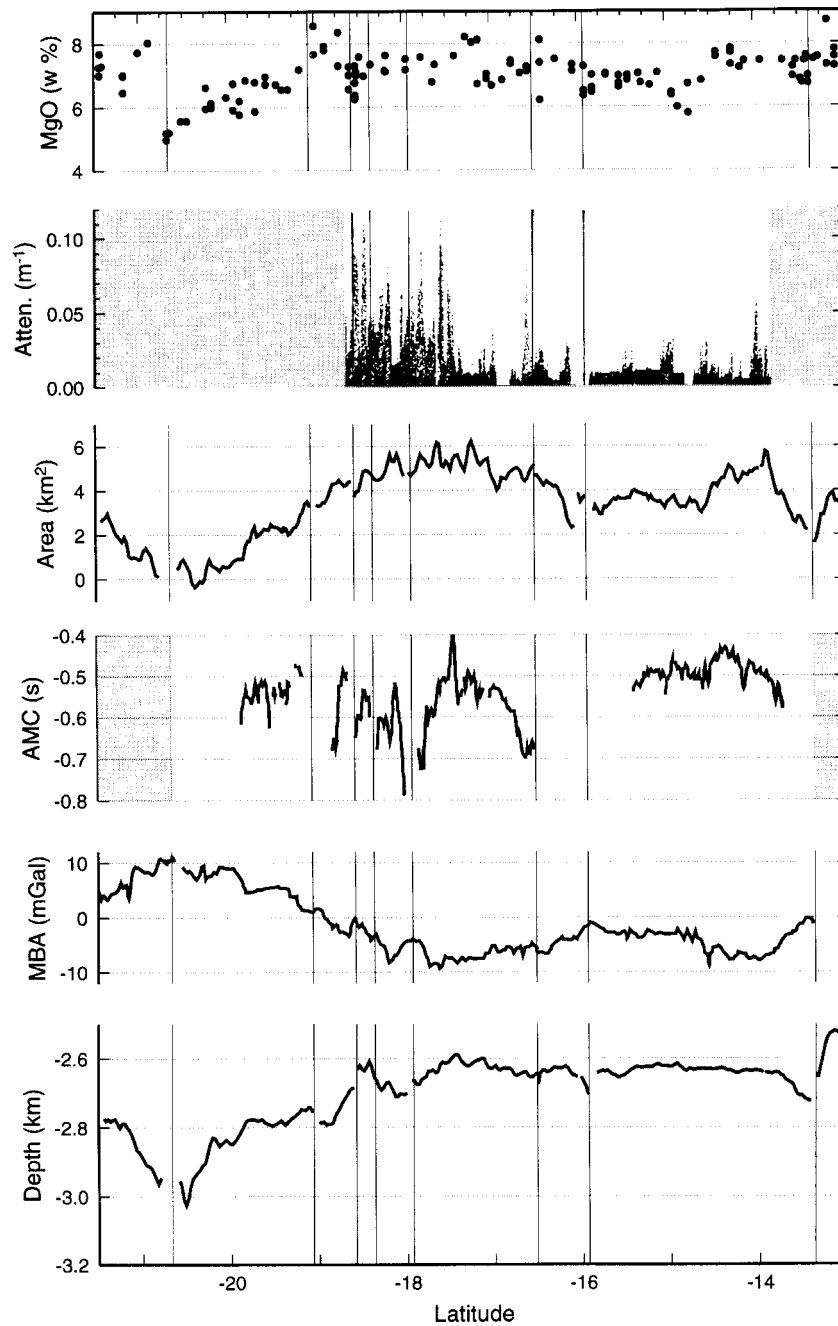


Figure 4. Along-axis variations of several parameters between Garrett transform and Easter microplate. From bottom to top, parameters are zero-age depths (Scheirer & Macdonald 1993), mantle Bouguer gravity anomalies (Cormier *et al.* 1995; Magde *et al.* 1995), subseafloor two-way travel times to the axial magma chamber seismic reflector (Detrick *et al.* 1993), cross-sectional area of the ridge axis (Scheirer & Macdonald 1993), light attenuation anomalies caused by suspended hydrothermal precipitates (Baker 1996), and MgO number for normal basalts (Sinton *et al.* 1991). Vertical lines mark the location of axial discontinuities with offset greater than 2 km. Shaded intervals indicate data gaps.

lines actually show a tendency for the extrusive layer to be thinner where the axial high is most inflated (Mutter *et al.* 1995; Carbotte *et al.* 1996; Tolstoy *et al.* 1996). This counter-intuitive relation can be explained if erupted lavas were more fluid (hotter) where the ridge is more inflated and ponded several kilometres off-axis rather than within the axial summit caldera (Hooft *et al.* 1996). The axial high seems to inflate in response to the size of the subcrustal mass anomaly rather than shallow crustal processes (Scheirer & Macdonald 1993; Wang & Cochran 1993): larger cross-sectional areas would reflect the presence of a subcrustal column of partial melt which is taller, wider or with a higher melt content. As a general rule, the cross-sectional area decreases toward segment ends (figure 4). The  $18^{\circ} 35' - 19^{\circ} 04' S$  and the  $19^{\circ} 04' - 20^{\circ} 40' S$  segments are notable exceptions to this rule. Both are shallowest and widest at their northern ends and plunge toward their southern ends. The former segment has initiated within the  $18^{\circ} 35' S$  OSC less than 40 000 yr ago and has since propagated southward at rates exceeding  $1000 \text{ mm yr}^{-1}$  (Cormier & Macdonald 1994); Conversely, the latter segment is retreating at the same rate from its northern end, and terminates into the large  $20^{\circ} 40' S$  OSC at its southern end. This recent, transient behaviour of the two segments probably accounts for their unusual characteristics.

Based on isotopic data and minor element ratios of basaltic glasses, Sinton *et al.* (1991) and Mahoney *et al.* (1994) propose that the three sections of the ridge bounded by the Garrett transform, the  $16^{\circ} S$  OSC, the  $20^{\circ} 40' S$  OSC and the northern boundary of the Easter microplate have distinct mantle source compositions. This primary magmatic segmentation happens to correspond to the long-wavelength variations in cross-sectional area (figure 4). Higher MgO content of basaltic glasses, which is thought to reflect higher temperatures of erupted basalts, also correlates well with the long-wavelength variations in cross-sectional area (Scheirer & Macdonald 1993). A similar relationship between mean MgO content and axial width was noted earlier for the northern EPR (Langmuir *et al.* 1986). Isotopic variations between  $16 - 20^{\circ} 40' S$  define a broad peak which may reflect the recent entry of a mantle plume or mantle heterogeneity beneath the ridge at  $17 - 17^{\circ} 30' S$  (Mahoney *et al.* 1994; Bach *et al.* 1994). Accordingly, ridge segments have propagated away from  $17 - 17^{\circ} 30' S$  since 1 Ma, and  $16^{\circ} 30' - 20^{\circ} 40' S$  corresponds to the outer limit of this propagation pattern (Cormier *et al.* 1996). While there exists a good correlation between first-order tectonic and magmatic segmentations, the existence of such a correlation for the finer scale segmentation is open to discussion. Based on glass compositional variations, Sinton *et al.* (1991) propose that OSCs and some other minor discontinuities define segments with distinct parental magma composition. In contrast, Bach *et al.* (1994) argue that melting conditions are basically uniform between  $13$  and  $18^{\circ} S$ .

Hydrothermal vents have been detected in most submersible dives (Renard *et al.* 1984; Auzende *et al.* 1996), towed camera surveys (Bäcker *et al.* 1985; Morton & Ballard 1986; Macdonald *et al.* 1988b; Sinton *et al.* 1991) and hydrographic tow-yos (Urabe *et al.* 1995; Baker & Urabe 1996) carried out along the southern EPR, attesting to the high level of hydrothermal activity at ultrafast spreading rates. Hydrothermal plume incidence is generally higher along portions of the ridge crest with inflated cross-sectional areas (figure 4), suggesting that hydrothermal circulation is more vigorous where the volume of interstitial melt in the mantle is high (Baker & Urabe 1996).

The two-way travel time to the AMC reflector is highly variable (figure 4). Near OSCs, the increasing two-way travel time to the AMC is probably an artifact of a

wandering ship track and of the high lateral velocity variations in the shallow crust near axis (Harding *et al.* 1993; Kent *et al.* 1993). Nonetheless, where additional control is provided by cross-axis profiles or away from OSCs, the depth to the AMC varies along-axis by up to 0.6–0.8 km (assuming an average velocity for the upper crust of 4.5–5 km s<sup>-1</sup>), an order of magnitude more than the corresponding seafloor depths. A strong AMC reflector is systematically detected along sections of the ridge with large cross-sectional areas (Scheirer & Macdonald 1993). Between Garrett transform and 16° S, the depth to the AMC correlates well with the cross-sectional area of the ridge. However, this simple relationship does not really apply elsewhere. For instance, a shallow AMC reflector is present between 19 and 20° S, where the ridge crest is relatively deep and narrow (figure 4).

The mantle Bouguer anomaly (MBA), which is the gravity anomaly corrected for the effect of bathymetry, of a constant crustal thickness and density, is inversely correlated to the axial volume (Scheirer & Macdonald 1993, and figure 4). Lower values of the MBA are indicative of a relative mass deficiency, and are generally interpreted to reflect the presence of a thicker crustal section, or excess heat and melt in the subaxial crust and mantle. MBA values increase toward the Wilkes transform fault, the Garrett transform fault, and the large 20° 40' S OSC (Wang & Cochran 1993; Magde *et al.* 1995; Cormier *et al.* 1995), suggesting that the magma supply is relatively starved in their vicinity. Small OSCs are generally not associated with any detectable MBA anomalies. Overall, the amplitude of the MBA variations is significantly smaller along the EPR (10–20 mgal) than those present along the slow spreading Mid-Atlantic Ridge (20–80 mgal) (Lin & Phipps Morgan 1992).

The fluctuations of the above parameters are good indicators of the magmatic budget of the EPR (Langmuir *et al.* 1986; Macdonald & Fox 1988; Scheirer & Macdonald 1993; Baker 1996). Shallow axial depths, large cross-sectional areas, high hydrothermal plume incidence, strong AMC reflectors, high MgO content of the glass and low residual gravity anomalies all correspond to a robust magmatic budget, such as occurs between 16° 30' and 19° S. The opposite trends, such as are present between 19° 30' and 21° 30' S, are indicators of a starved magmatic budget. Present magmatic regimes of the EPR seem to be long-lived, as revealed by the constancy of several parameters along flow lines for up to a few million years. Narrow axial highs are systematically flanked by blocky lineated abyssal hills, and broad axial highs by smoother abyssal hill terrain (Cochran *et al.* 1993; Goff *et al.* 1993; Cormier *et al.* 1994). Smoother seafloors are thought to result from the combined effects of blanketing by voluminous lava flows issued from the ridge axis (Macdonald *et al.* 1996) and lower fault throws developing in areas where the crust is hotter, leading to a thinner brittle layer (Goff *et al.* 1993; Carbotte & Macdonald 1994). Careful rock sampling across the northern EPR indicates that where the ridge is magmatically robust, the temperatures of eruption remained nearly constant since 0.8 Ma, and that where the ridge is magmatically starved, the temperature of erupted magma changes significantly with time (Batiza *et al.* 1996). This is interpreted to indicate that magmatically robust ridges have steady state magma chambers, whereas magmatically starved ridges have smaller, transient magma chambers. Finally, the broad, high residual gravity anomalies associated with the slowly migrating 20° 40' S OSC persist off-axis for at least 2 my, indicating that a starved regime has persisted at this OSC during that entire time interval (Cormier *et al.* 1995). Ridge propagation events are expected to disrupt flow-line trends, and their associated oblique discordant zones

on the ridge flank may sometimes correspond to boundaries between seafloors with opposing characteristics.

### 7. Accretionary processes along the ultrafast EPR: two or three dimensional?

Two extreme models of mantle upwelling pattern could explain the relatively uniform characteristics of the EPR (Lin & Phipps Morgan 1992; Bell & Buck 1992). Mantle could be upwelling somewhat evenly beneath the ridge axis, in a two-dimensional or 'sheet-like' pattern. Alternatively, mantle could be upwelling at discrete intervals along the ridge axis and the magma being transported efficiently along-axis within the crust and upper mantle, forming a three-dimensional or 'plume-like' pattern. Mantle upwelling could also assume any pattern intermediate to these two or three-dimensional models. Which style of mantle upwelling actually feeds fast spreading ridges is still debatable, the following sections review the arguments for and against each model.

#### (a) Arguments in favour of uniform accretion

The concept of two-dimensional accretion at the fast spreading EPR initiated from comparing the variations of its axial characteristics (figure 4) to those of the slow-spreading Mid-Atlantic Ridge (Lin & Phipps Morgan 1992). Although many of the characteristics of the MAR display the same trends as those of the EPR with respect to tectonic segmentation, their variations are not only more systematic, they also have much larger magnitudes. Along the MAR, the ridge axis deepens by 700–1700 m and the residual gravity anomalies increase by 20–80 mGal toward transform faults, while the crustal thickness is often a few kilometres thinner beneath the transform faults (White *et al.* 1984; Lin *et al.* 1992; Detrick *et al.* 1995). The strong correlation between axial characteristics and axial segmentation of the MAR is commonly thought to reflect the three-dimensional geometry of mantle and magma circulation beneath the ridge. Magma supply is inferred to be focused beneath the shallower part of the ridge axis near mid-segment, and transform faults to mark the distal extremities of the magmatic segments. This model predicts that the magmatic budget will change from robust near mid-segment to relatively starved near ridge-transform intersection, consistent with the observations along the MAR (White *et al.* 1984; Cannat *et al.* 1995). By contrast, the smoothly varying EPR characteristics suggest that magma supply is more homogenous.

Satellite altimetry data reveal that the seafloor created at the EPR singularly lacks the 'crenulated' appearance of the seafloor created at slower spreading ridges (Phipps Morgan & Parmentier 1995). 'Crenulations' are regularly spaced gravity lineations in the spreading direction, which reflect the stationary segmentation of the ridge axis over long periods of time. The absence of crenulations along the EPR could result from an essentially two-dimensional mantle flow structure (Phipps Morgan & Parmentier 1995). Accordingly, numerical experiments indicate that with increasing spreading rates, passive upwelling will eventually prevail over buoyant upwelling (Parmentier & Phipps Morgan 1990; Lin & Phipps Morgan 1992; Sparks & Parmentier 1993; Jha *et al.* 1994; Kincaid *et al.* 1996). Passive upwelling is that induced by the separation of the plates, and is predicted to be mostly uniform along a ridge segment (Phipps Morgan & Forsyth 1988). Buoyant active upwelling initiates as along-axis instabilities in the mantle, and is enhanced by the lowered densities of

the thermally expanded, depleted mantle and of the retained melt within the mantle matrix. Whether buoyant upwelling is a cause or a consequence of the segmentation still remains to be determined.

The axial high stands 200–300 m higher than predicted by simple conductive cooling of the lithosphere with age (Madsen *et al.* 1984; Wilson 1992). Detailed, two-dimensional analysis of both gravity and bathymetric data indicate that the magma chamber contributes negligibly to these anomalous bathymetry signals; on the other hand, the gravity signal of the axial region is well accounted for by the thermal structure of the crust and shallow mantle (Madsen *et al.* 1990; Wilson 1992; Wang & Cochran 1993; Magde *et al.* 1995; Wang *et al.* 1996). These studies suggest that the axial high is isostatically compensated by a low density body located below the crust. By taking into account some realistic thermal models for the lithosphere and asthenosphere, this compensating body is estimated to be narrower than 10 km and taller than 20 km (Wilson 1992; Wang & Cochran 1993; Magde *et al.* 1995). If this low density body represented a column of partial melt feeding the ridge axis, a melt fraction of 1–3% would imply a column at least 30 km tall. Because an axial high is a ubiquitous feature along the EPR, the above gravity studies imply that a tall column of partial melt underlies the entire length of the ridge axis, consistent with a two-dimensional model for mantle upwelling. Nonetheless, the width and height of that column and its melt content would need to vary along-axis in accordance with the varying depth and cross-sectional area of the axial high, and with its varying MBA (Wang & Cochran 1993).

If all axial discontinuities represented the distal ends of a three-dimensional magmatic plumbing system, intuition would predict a decrease in extrusive thickness in their vicinities. Yet, two-way travel times to the base of seismic layer 2A, interpreted to correspond to the base of the extrusive layer, do not vary in any systematic way near a *ca.* 1 km offset of the EPR at 14° 27' S (Kent *et al.* 1994). This suggests that minor offsets of the ridge axis do not correspond to long-term reduction in magma supply, and are probably ‘transparent’ features in terms of mantle upwelling. Accordingly, smaller offsets are generally not associated with any recognizable ‘scars’ on the rise flanks, implying that most of them are transient, surficial features of the plate boundary (Macdonald *et al.* 1988a) or that they migrate too rapidly to generate easily detected discordant zones (Cormier & Macdonald 1994). Furthermore, the small OSCs between 18° 15' and 20° S are not associated with any significant residual MBA (figure 4), as would be expected if they were associated with a long-lived segmentation in mantle upwelling (Cormier *et al.* 1995).

(b) *Arguments in favour of large scale along-axis magma transport*

The common occurrence of ridge propagation events along the southern EPR, as summarized above, attests to one form of along-strike magma transport. Based on detailed studies at propagator tips, spreading centres seem to lengthen initially by tectonic rupture of the older lithosphere, extrusive volcanism following at a later stage only (Kleinrock *et al.* 1989; Naar *et al.* 1991). This progression toward full seafloor spreading suggests that, at least initially, magma is being transported along-strike toward the propagator tip rather than being fed vertically from the mantle. Large scale propagation events often occur with average sustained rates comparable to the half spreading rates, or higher. For instance, the west ridge of the Bauer microplate propagated northward *ca.* 1000 km sometime between 10 and 5 Ma (Lonsdale 1989), yielding a conservative estimate for its mean propagation rate of 200 mm yr<sup>-1</sup>. The

large 29° S OSC averages a net propagation rate of 120 mm yr<sup>-1</sup> since 2 Ma (Korenaga & Hey 1996). Since 1 Ma, a large OSC has propagated southward between 17–19° S at 200–1000 mm yr<sup>-1</sup> (Cormier *et al.* 1996). Through propagation, magmatic segments lengthen or shorten through time, implying that underlying mantle upwelling patterns are unstable on the same time scale. Hence, the absence of spreading-parallel crenulations in the altimetry data on the EPR flanks may reflect the frequency of ridge propagation events rather than the two dimensionality of mantle upwelling (Phipps Morgan & Parmentier 1995).

While recent gravity analyses argue for the existence of a continuous column of partial melt beneath the ridge axis, they also imply that the melt content, width or height of that column must vary significantly along axis. Although axial depths are constant between 7° 12' and 8° 38' S, the changes in cross-sectional area and MBA requires that the mass deficiency beneath the central section is 20–60% more than near segment ends (Wang & Cochran 1993). Similarly, axial depths vary little between 13° 30' and 17° 56' S, yet MBA variations imply the presence of a hotter crust or greater amount of interstitial melt at 17° 20' S than at 14° 15' S (Magde *et al.* 1995). The constant axial depth along sections of the EPR requires the presence of an efficient shallow magmatic plumbing system that extends the length of these ridge segments and redistributes the magma evenly (Wang & Cochran 1993).

Magma supply seems slightly lower in the vicinity of large axial discontinuities, in agreement with them marking the distal ends of an efficient magmatic plumbing system. Hence, while axial depths remain constant as the Garrett transform fault is approached from the south, the axial magma chamber progressively deepens by about 240 m over a 60 km distance (Tolstoy *et al.* 1996). Interpretation of gravity anomalies over the ridge axis and its flanks indicates that a crust about 500 m thinner than typical has been consistently accreted near the large 20° 40' S OSC since 2 Ma (Cormier *et al.* 1995).

Topography and gravity signals along the ultra-slow spreading Reykjanes Ridge display the same subdued fluctuations as the EPR (Bell & Buck 1992). Because the crust of the Reykjanes Ridge is much thicker than typical, its lower section may be reaching temperatures as high as those beneath the EPR. This suggests that mantle upwelling may be diapiric at all spreading rates, but that wherever the lower crust is hot enough, it undergoes rapid ductile flow which evens out any significant crustal thickness variations (Bell & Buck 1992).

Two-way travel time variations to the seismic moho are interpreted as crustal thickness variations of up to 2.6 km at 9–10° N along the EPR (Barth & Mutter 1996). Counter to conventional wisdom, the thinnest crust seems to coincide with the lowest MBA values and minimum axial depth (Wang *et al.* 1996). A self-consistent interpretation of both the seismic and gravity data near 9–10° N is that mantle upwelling is focused beneath 9° 50' N and that through efficient along-axis transport, magma accumulates near the ends of the segment. However, moho reflections may arise from the top of the moho transition zone rather than from the crust–mantle boundary (Collins *et al.* 1986), and the variability in two-way travel time may reflect that of thickness of the magmatic crust only, rather than thickness of the crust plus transition zone. Accordingly, detailed mapping in the Oman ophiolite reveals that the thickest moho transition zones occur on top of mantle diapirs (Nicolas *et al.* 1996).

A seismic tomography experiment at 9° 30' N along the EPR reveals a local segmentation of the low velocity zone which is strikingly similar in extent and dimension

to the fine scale tectonic segmentation of the ridge (Toomey *et al.* 1990). This apparent thermal segmentation of the ridge is consistent with injection of mantle-derived melt midway along the 12 km long ridge segment. The small wavelength of this segmentation is also consistent with observations in ophiolites. Detailed mapping of the flow structures preserved in the peridotites of the Oman ophiolites, which are thought to have been accreted at a fast spreading ridge, reveals three-dimensional patterns with 10–20 km wavelength (Nicolas *et al.* 1994). These are interpreted as frozen-in mantle diapirs that fed the ridge axis before cessation of spreading and obduction.

## 8. Discussion and conclusions

Although models for two- or three-dimensional mantle upwelling beneath the EPR seem incompatible, evidence presented in support of each indicates that, to some extent, both can be active along the EPR. Which model best applies for a given area may depend on the observation scale, or on local fluctuations in melt supply and thermal structure of the ridge.

The variability in axial morphology and the ridge propagation patterns suggest that along-strike magma transport can occur and is directed away from the most inflated, most robust sections of the southern EPR (Wang & Cochran 1993; Cormier *et al.* 1996). However, how widespread lateral transport is as an accretionary mechanism remains to be constrained. If lateral melt flow were entirely confined within the crustal layer, simple-minded computations indicate that flow rates necessary to feed a ridge segment would be reasonable. For example, in the extreme case where the entire melt supply to a ridge segment would upwell in its centre, the maximum rate at which magma would need to flow along-axis to accommodate the accretion of a crust 6.5 km thick is directly proportional to the half segment length and the spreading rate, and inversely proportional to the cross-sectional area of the conduit through which magma travels. Hence, if flow were confined to a 500 m wide and 10 m thick melt lens, the maximum flow rate necessary to feed a 200 km long segment would be about  $2 \text{ m h}^{-1}$  above the locus of upwelling, and would decrease to zero toward segment ends. These rates seem feasible for mid-ocean ridge basalts, which are inferred to flow significantly faster along dikes (Dziak *et al.* 1995) and during eruptions (Griffiths & Fink 1992). If the conduit were extended to include the entire thickness of the crystal mush zone below the magma lens (about 2 km thick and 2 km wide), the maximum flow rate required for a 200 km long segment would drop to *ca.*  $25 \text{ m yr}^{-1}$  above the centre of upwelling, becoming stagnant near segment ends. This maximum rate is somewhat higher than documented ridge propagation rates along the southern EPR (up to  $1 \text{ m yr}^{-1}$ ), but is not unlikely for partially crystallized gabbros deforming ductilely near their rigidus temperature (Bell & Buck 1992).

Axial depth characteristics may reflect whether along-axis magma transport is vigorous or stagnant. Over the two long sections of ridge at  $7^\circ 12' - 8^\circ 38' \text{ S}$  and  $14 - 18^\circ \text{ S}$ , axial depths undulate by less than 50 m. This remarkable flatness suggests either efficient along-axis flow (Lonsdale 1989; Cochran *et al.* 1993), magmastic equilibrium (Sinton & Detrick 1992) or isostatic compensation over a uniform partial melt conduit 50–70 km tall (Magde *et al.* 1995). In contrast, only 2 km from the ridge crest in the same areas, seafloor depths fluctuate by a few hundred metres along-strike. The very narrowness of the zone of flat topography suggests that the controlling process is a shallow one, probably occurring within the crust. Because the depth to the top of the AMC varies by 240–600 m between  $14 - 18^\circ \text{ S}$  (Detrick

*et al.* 1993; Mutter *et al.* 1995; Tolstoy *et al.* 1996), an order of magnitude higher than the axial depths, constant axial depths cannot result from efficient horizontal transport within the thin melt lens. Rather, magmatic equilibrium or lateral flow must occur within the lower crust, in the crystal mush zone that underlies the melt lens. Temperatures within this crystal mush zone are inferred to be near the rigidus, and slow magmatic flow could occur (Bell & Buck 1992; Sinton & Detrick 1992; Nicolas *et al.* 1993).

Although minor discontinuities are not associated with any large signal in the MBA or axial volume, they can represent significant barrier to along-axis flow. The 1.2 km offset at 8° 38' S marks the boundary between a ridge segment with constant axial depths to the north, and one with steadily decreasing axial depths to the south. Provided that constant axial depths reflect active ductile flow within the partially crystallized gabbros, the small 8° 38' S discontinuity would mark the southern extent of that process for this area. Accordingly, there is a jump in MgO content across the minor 14° 27' S discontinuities although the AMC appears continuous, suggesting it represents a mixing boundary within a continuous magma chamber (Sinton *et al.* 1991).

The existence of a tall column of partial melt feeding the entire EPR is not required by the gravity anomalies (Wilson 1992), and has been inferred because it could isostatically support the axial high (Madsen *et al.* 1984; Wilson 1992; Wang & Cochran 1993; Magde *et al.* 1995). Alternatively, the axial high may owe its existence to the dynamic moments acting in the axial region (Forsyth *et al.* 1994). The shallow magma chamber and frequent intrusion of dikes above the chamber may relieve the regional stresses, creating a weak zone at the top of the extending lithosphere. This would induce dynamic moments which tend to uplift the plate boundary. If this model for the origin of the axial high were correct rather than that of isostatic equilibrium, there would not be any requirements for the presence of a tall column of partial melt. Further evidence for or against the presence of a partial melt column beneath the EPR should come from analysis of the data acquired during the recent MELT experiment at 16–18° S, a large scale experiment designed precisely to address this problem (Forsyth & Chave 1994).

The following model is proposed, which could reconcile most observations. It is envisioned that mantle upwells vertically everywhere along the ridge axis, but that the intensity of this upwelling varies significantly both spatially and temporally. Larger volume of melt could be produced where 'easily melted' mantle heterogeneities are embedded within the asthenosphere (Wilson 1992). As the EPR migrates westward relative to the asthenosphere, such heterogeneities may be fed into the ridge axis somewhat randomly. Because the gabbros beneath the ridge crest are around their rigidus temperatures, minor temperature fluctuations might be sufficient to favour or inhibit their ductile flow. Where melt supply is locally abundant, gabbro temperatures would become higher than their rigidus, favouring along-axis flow toward regions with lower melt supply. On occasion, gabbros may be hot enough and contain sufficient amount of interstitial melt to allow magmatic equilibrium or efficient along-axis flow, resulting in a subhorizontal ridge crest. Where melt supply becomes particularly robust, lateral flow may be sufficiently vigorous to allow propagation across large ridge offsets. In contrast, locally cooler mantle or low melt supply will result in gabbro temperatures remaining below their rigidus, implying a sluggish or non-existent along-axis flow.

I thank Joe Cann and Harry Eldefield for having motivated this paper. I am indebted to Ken

Macdonald for introducing me to the southern EPR and for many interesting discussions. This paper benefited from insightful remarks by John Mutter and Bill Menke. Lamont–Doherty Earth Observatory contribution # 5546.

### References

- Atwater, T. & Severinghaus, J. 1989 Tectonic maps of the northeast Pacific. In *The geology of North America, the East Pacific Ocean and Hawaii* (ed. E. L. Winterer, D. M. Hussong & R. W. Decker), vol. N, pp. 15–20. Geological Society of America.
- Auzende, J.-M., Hey, R. N., Pelletier, B., Rouland, D., Lafoy, Y., Gracia, E. & Huchon, P. 1995 Propagating rift west of the Fiji Archipelago (North Fiji Basin, SW Pacific). *J. Geophys. Res.* **100**, 17 823–17 835.
- Auzende, J.-M., Ballu, V., Batiza, R., Bideau, D., Charlou, J.-L., Cormier, M.-H., Fouquet, Y., Geistdoerfer, P., Lagabrielle, Y., Sinton, J. & Spadea, P. 1996 Recent tectonic, magmatic and hydrothermal activity on the East Pacific Rise between 17° and 19° S: submersible observations. *J. Geophys. Res.* **101**, 17 995–18 010.
- Bach, W., Hegner, E., Erzinger, J. & Satir, M. 1994 Chemical and isotopic variations along the superfast spreading East Pacific Rise from 6° to 30° S. *Contr. Miner. Petr.* **116**, 365–380.
- Bäcker, H., Lange, J. & Marchig, V. 1985 Hydrothermal activity and sulfide formation in axial valleys of the East Pacific Rise crest between 18° and 22° S. *Earth Planet. Sci. Lett.* **72**, 9–22.
- Baker, E. T. & Urabe, T. 1996 Extensive distribution of hydrothermal plumes along the superfast spreading East Pacific Rise, 13° 30′–18° 40′ S. *J. Geophys. Res.* **101**, 8685–8695.
- Baker, E. T. 1996 Geological indexes of hydrothermal venting. *J. Geophys. Res.* **101**, 13 741–13 753.
- Barth, G. A. & Mutter, J. C. 1996 Variability in oceanic crustal thickness and structure: Multi-channel seismic reflection results from the East Pacific Rise, 8° 50′ N to 9° 50′ N and 12° 30′ N to 13° 30′ N. *J. Geophys. Res.* **101**, 17 951–17 975.
- Batiza, R., Niu, Y., Karsten, J. L., Potts, E., Norby, L. & Buttler, R. 1996 Steady and non-steady magma chambers below the East Pacific Rise. *Geophys. Res. Lett.* **23**, 221–224.
- Bell, R. E. & Buck, W. R. 1992 Crustal control of ridge segmentation inferred from observations of the Reykjanes Ridge. *Nature* **357**, 583–586.
- Bicknell, J. D., Sempère, J.-C., Macdonald, K. C. & Fox, P. J. 1987 Tectonics of a fast spreading centre: a Deep-Tow and Sea Beam survey on the East Pacific Rise at 19° 30′ S. *Mar. Geophys. Res.* **9**, 25–46.
- Bird, R. T. & Naar, D. F. 1994 Intratransform origins of mid-ocean ridge microplates. *Geology* **22**, 987–990.
- Bird, R. T., Naar, D. F., Larson, R. L., Searle, R. C. & Scotese, C. R. 1997 Plate tectonic reconstructions of the Juan Fernandez microplate: transformation from internal shear to rigid rotation. *J. Geophys. Res.* (Submitted.)
- Cannat, M., Mével, C., Maia, M., Deplus, C., Durand, C., Gente, P., Agrinier, P., Belarouchi, A., Dubuisson, G., Humler, E. & Reynolds, J. 1995 Thin crust, ultramafic exposures, and rugged faulting patterns at the Mid-Atlantic Ridge (22°–24° N). *Geology* **23**, 49–52.
- Carbotte, S. M. & Macdonald, K. C. 1994 Comparison of sea floor tectonic fabric created at intermediate, fast, and superfast spreading ridges: influence of spreading rate, plate motions and ridge segmentation on fault patterns. *J. Geophys. Res.* **99**, 13 609–13 631.
- Carbotte, S. M., Mutter, J. C. & Xu, L. 1997 Contribution of tectonism and volcanism to axial and flank morphology of the southern EPR, 17° 10′–17° 40′, from a study of layer 2A geometry. *J. Geophys. Res.* (In the press.)
- Caress, D. W., Burnett, M. S. & Orcutt, J. A. 1992 Tomographic image of the axial low velocity zone at 12° 50′ N on the East Pacific Rise. *J. Geophys. Res.* **97**, 9243–9263.
- Charlou, J. L., Fouquet, Y., Donval, J.-P., Auzende, J.-M., Jean-Baptiste, P., Stievenard, M. & Michel, S. 1996 Mineral and gas chemistry of hydrothermal fluids on an ultrafast spreading ridge: East Pacific Rise, 17°–19° S (Naudur cruise 1993) phase separation processes controlled by volcanic and tectonic activity. *J. Geophys. Res.* **101**, 15 899–15 919.

- Chen, Y. J. 1992 Oceanic crustal thickness versus spreading rate. *Geophys. Res. Lett.* **19**, 753–756.
- Cochran, J. R. 1986 Variations in subsidence rates along intermediate and fast spreading mid-ocean ridges. *Geophys. J. R. Astr. Soc.* **87**, 421–454.
- Cochran, J. R., Goff, J. A., Malinverno, A., Fornari, D. J., Keeley, C. & Wang, X. 1993 Morphology of a 'superfast' mid-ocean ridge crest and flanks: the East Pacific Rise 7°–9° S. *Mar. Geophys. Res.* **15**, 65–75.
- Collins, J. A., Brocher, T. M. & Karson, J. A. 1986 Two-dimensional seismic reflection modeling of the inferred fossil oceanic crust/mantle transition in the Bay of Islands ophiolite. *J. Geophys. Res.* **91**, 12 520–12 538.
- Cormier, M.-H. & Macdonald, K. C. 1994 East Pacific Rise 18°–19° S: asymmetric spreading and ridge reorientation by ultra-fast migration of axial discontinuities. *J. Geophys. Res.* **99**, 543–564.
- Cormier, M.-H., Macdonald, K. C. & Wilson, D. S. 1995 A three-dimensional gravity analysis of the East Pacific Rise, 18°–21° 30' S. *J. Geophys. Res.* **100**, 8063–8082.
- Cormier, M.-H., Scheirer, D. S. & Macdonald, K. C. 1996 Evolution of the East Pacific Rise at 16°–19° S since 5 Ma: bisection of overlapping spreading centres by new, rapidly propagating ridge segments. *Mar. Geophys. Res.* **18**, 53–84.
- DeMets, C., Gordon, R. G., Argus, D. F. & Stein, S. 1994 Effect of recent revisions to the geomagnetic reversal time scale on estimates of current plate motions. *Geophys. Res. Lett.* **21**, 2191–2194.
- Detrick, R. S., Harding, A. J., Kent, G. M., Orcutt, J. A., Mutter, J. C. & Buhl, P. 1993 Seismic structure of the southern East Pacific Rise. *Science* **259**, 499–503.
- Detrick, R. S., Needham, H. D. & Renard, V. 1995 Gravity anomalies and crustal thickness variations along the Mid-Atlantic Ridge between 33° N and 40° N. *J. Geophys. Res.* **100**, 3767–3787.
- Dziak, R. P., Fox, C. G. & Schreiner, A. E. 1995 The June–July 1993 seismo-acoustic event at CoAxial segment, Juan de Fuca Ridge: evidence for a lateral dike injection. *Geophys. Res. Lett.* **22**, 135–138.
- Forsyth, D. W. & Chave, A. D. 1991 Experiment investigates magma in the mantle beneath mid-ocean ridge. *Eos* **75**, 537–540.
- Forsyth, D. W., Eberle, M. A. & Parmentier, E.M. 1994 An alternative explanation for the origin of the axial high on fast spreading ridges. *Eos* **75**, 640 (abstract).
- Fox, P. J. & Gallo, D. J. 1989 Transforms of the eastern central Pacific. In *The Geology of North America, the Eastern Pacific Ocean and Hawaii*, vol. N, pp. 111–124. Geological Society of America.
- Francheteau, J. & Ballard, R. D. 1983 The East Pacific Rise near 21° N, 13° N and 20° S: inferences for along-strike variability of axial processes of the mid-ocean ridge. *Earth Planet. Sci. Lett.* **64**, 93–116.
- Francheteau, J., Yelles-Chaouche, A. & Craig, H. 1987 The Juan Fernandez microplate north of the Pacific-Nazca-Antarctic plate junction at 35° S. *Earth Planet. Sci. Lett.* **86**, 253–268.
- Francheteau, J., Patriat, P., Segoufin, J., Armijo, R., Doucoure, M., Yelles-Chaouche, A., Zúkin, J., Calmant, S., Naar, D. F. & Searle, R. 1988 Pito and Orongo fracture zones: the northern and southern boundaries of the Easter microplate (southeast Pacific). *Earth Planet. Sci. Lett.* **89**, 363–374.
- Gente, P., Pockalny, R. A., Durand, C., Deplus, C., Maia, M., Ceuleneer, G., Mèvel, C., Cannat, M. & Laverne, C. 1995 Characteristics and evolution of the segmentation of the Mid-Atlantic Ridge between 20° N and 24° N during the last 10 million years. *Earth Planet. Sci. Lett.* **129**, 55–71.
- Goff, J. A., Malinverno, A., Fornari, D. J. & Cochran, J. R. 1993a Abyssal hills segmentation—quantitative analysis of the East Pacific Rise flanks 7° S–9° S. *J. Geophys. Res.* **98**, 13 851–13 862.
- Goff, J. A., Fornari, D. J., Cochran, J. R., Keeley, C. & Malinverno, A. 1993b Wilkes transform system and 'nannoplate'. *Geology* **21**, 623–626.

- Griffiths, R. W. & Fink, J. H. 1992 Solidification and morphology of submarine lavas: a dependence on extrusion rate. *J. Geophys. Res.* **97**, 19 729–17 737.
- Gripp, A. E. & Gordon, R. G. 1990 Current plate velocities relative to the hot spots incorporating the NUVEL-1 global plate motion model. *Geophys. Res. Lett.* **17**, 1109–1112.
- Harding, A. J., Orcutt, J. A., Kappus, M. E., Vera, E. E., Mutter, J. C., Buhl, P., Detrick, R. S. & Brocher, T. M. 1989 Structure of young oceanic crust at 13° N on the East Pacific Rise from expanding spread profiles. *J. Geophys. Res.* **94**, 12 163–12 196.
- Henstock, T. J., Woods, A. W. & White, R. S. 1993 The accretion of oceanic crust by episodic sill injection. *J. Geophys. Res.* **98**, 4143–4161.
- Hey, R., Duennebieer, F. K. & Morgan, W. J. 1980 Propagating rifts on mid-ocean ridges. *J. Geophys. Res.* **85**, 3647–3658.
- Hey, R. N., Johnson, P. D., Martinez, F., Korenaga, J., Somers, M. L., Huggett, Q. J., LeBas, T. P., Rusby, R. I. & Naar, D. F. 1995 Plate boundary reorganization at a large-offset, rapidly propagating rift. *Nature* **378**, 167–170.
- Holler, G., Marchig, V. & the shipboard scientific party 1990 Hydrothermal activity on the East Pacific Rise: stages of development. *Geol. J* **75**, 3–22.
- Hooft, E. E., Schouten, H. & Detrick, R. S. 1996 Constraining crustal emplacement processes from the variation in seismic layer 2A thickness at the East Pacific Rise. *Earth Planet. Sci. Lett.* **142**, 289–309.
- Hussenoeder, S. A., Collins, J. A., Kent, G. M., Detrick, R. S. & the TERA Group 1996 Seismic analysis of the axial magma chamber reflector along the southern East Pacific Rise from conventional reflection profiling. *J. Geophys. Res.* **101**, 22087–22105.
- Jha, K., Parmentier, E. M. & Phipps Morgan, J. 1994 The role of mantle-depletion and melt-retention buoyancy in spreading-centre segmentation. *Earth Planet. Sci. Lett.* **125**, 221–234.
- Kent, G. M., Harding, A. J. & Orcutt, J. A. 1990 Evidence for a smaller magma chamber beneath the east Pacific Rise at 9° 30' N. *Nature* **344**, 650–663.
- Kent, G. M., Harding, A. J. & Orcutt, J. A. 1993 Distribution of magma beneath the east Pacific Rise between the Clipperton transform and the 9° 17' N deval from forward modeling of common depth point data. *J. Geophys. Res.* **98**, 13 945–13 969.
- Kent, G. M., Harding, A. J., Orcutt, J. A., Detrick, R. S., Mutter, J. C. & Buhl, P. 1994 Uniform accretion of oceanic crust south of the Garrett transform at 14° 15' S on the East Pacific Rise. *J. Geophys. Res.* **99**, 9097–9116.
- Kincaid, C., Sparks, D. W. & Detrick, R. S. 1996 The relative importance of plate-driven and buoyancy-driven flow at mid-ocean ridges. *J. Geophys. Res.* **101**, 16 177–16 193.
- Klaus, A., Icaý, W., Naar, D. & Hey, R. N. 1991 SeaMARC II survey of a propagating limb of a nontransform offset near 29° S along the fastest spreading East Pacific Rise segment. *J. Geophys. Res.* **96**, 9985–9998.
- Kleinrock, M. C. & Hey, R. N. 1989 Detailed tectonics near the tip of the Galapagos 95.5° W propagator: how the lithosphere tears and a spreading axis develops. *J. Geophys. Res.* **94**, 13 801–13 838.
- Korenaga, J. & Hey, R. N. 1996 Recent dueling propagation history at the fastest spreading centre, the East Pacific Rise, 26°–32° S. *J. Geophys. Res.* **101**, 18 023–18 041.
- Langmuir, C. H., Bender, J. F. & Batiza, R. 1986 Petrological and tectonic segmentation of the East Pacific Rise, 5° 30'–14° 30' N. *Nature* **322**, 422–429.
- Larson, R. L., Searle, R. C., Kleinrock, M. C., Schouten, H., Bird, R. T., Naar, D. F., Rusby, R. I., Hooft, E. E. & Lasthiotakis, H. 1992 Roller-bearing tectonic evolution of the Juan Fernandez microplate. *Nature* **356**, 571–576.
- Lin, J., Purdy, G. M., Schouten, H., Sempère, J.-C. & Zervas, C. 1990 Evidence from gravity data for focused magmatic accretion along the Mid-Atlantic ridge. *Nature* **344**, 627–632.
- Lin, J. & Phipps Morgan, J. 1992 The spreading rate dependence of three-dimensional mid-ocean ridge gravity structure. *Geophys. Res. Lett.* **19**, 13–16.
- Lonsdale, P. 1983 Overlapping rift zones at the 5.5° S offset of the East Pacific Rise. *J. Geophys. Res.* **88**, 9393–9406.
- Lonsdale, P. 1988 Structural pattern of the Galapagos microplate and evolution of the Galapagos triple junctions. *J. Geophys. Res.* **93**, 13 551–13 574.

- Lonsdale, P. 1989 Segmentation of the Pacific-Nazca spreading centre, 1° N–20° S. *J. Geophys. Res.* **94**, 12 197–12 226.
- Lonsdale, P. 1994 Geomorphology and structural segmentation of the crest of the southern (Pacific–Antarctic) East Pacific Rise. *J. Geophys. Res.* **99**, 4683–4702.
- Macdonald, K. C. 1982 Mid-ocean ridges: fine scale tectonic, volcanic and hydrothermal processes within the plate boundary zone. *Ann. Rev. Earth Planet. Sci.* **10**, 155–190.
- Macdonald, K. C., Sempère, J.-C. & Fox, P. J. 1984 East Pacific Rise from Siqueiros to Orozco fracture zones: along-strike continuity of axial neovolcanic zone and structure and evolution of overlapping spreading centres. *J. Geophys. Res.* **89**, 6049–6069.
- Macdonald, K. C., Fox, P. J., Perram, L. J., Eisen, M. F., Haymon, R. M., Miller, S. P., Carbotte, S. M., Cormier, M.-H. & Shor, A. N. 1988a A new view of the mid-ocean ridge from the behaviour of ridge axis discontinuities. *Nature* **335**, 217–225.
- Macdonald, K. C., Haymon, R. M., Miller, S. P. & Sempère, J.-C. 1988b Deep-tow and sea beam studies of dueling propagating ridges on the East Pacific Rise near 20° 40' S. *J. Geophys. Res.* **93**, 2875–2898.
- Macdonald, K. C. & Fox, P. J. 1988 The axial summit graben and cross-sectional shape of the East Pacific Rise as indicators of axial magma chambers and recent volcanic eruptions. *Earth Planet. Sci. Lett.* **88**, 119–131.
- Macdonald, K. C., Scheirer, D. S. & Carbotte, S. M. 1991 Mid-ocean ridges: discontinuities, segments and giant cracks. *Science* **253**, 986–994.
- Madsen, J. A., Forsyth, D. W. & Detrick, R. S. 1984 A new isostatic model for the East Pacific Rise crest. *J. Geophys. Res.* **89**, 9997–10015.
- Madsen, J. A., Detrick, R. S., Mutter, J.-C., Buhl, P. & Orcutt, J. A. 1990 A two and three-dimensional analysis of gravity anomalies associated with the East Pacific Rise at 9° N and 13° N. *J. Geophys. Res.* **95**, 4967–4987.
- Magde, L. S., Detrick, R. S. & the TERA group 1995 Crustal and upper mantle contribution to the axial gravity anomaly at the southern East Pacific Rise. *J. Geophys. Res.* **100**, 3747–3766.
- Mahoney, J. J., Sinton, J. M., Macdougall, J. D., Spencer, K. J. & Lugmair, G. W. 1994 Isotope and trace element characteristics of a superfast spreading ridge: East Pacific Rise, 13–23° S. *Earth Planet. Sci. Lett.* **121**, 173–193.
- Marsh, B. D. 1989 Magma chambers. *A. Rev. Earth Planet. Sci.* **17**, 439–474.
- Morton, J. L. & Ballard, R. D. 1986 East Pacific Rise at latitude 19° S: evidence for a recent ridge jump. *Geology* **14**, 111–114.
- Mutter, J. C., Carbotte, S. M., Su, W., Xu, L., Buhl, P., Detrick, R. S., Kent, G. M., Orcutt, J. A. & Harding, A. J. 1995 Seismic images of active magma systems beneath the East Pacific Rise between 17° 05' and 17° 35' S. *Science* **268**, 391–395.
- Naar, D. F. & Hey, R. N. 1989a Speed limit for oceanic transform faults. *Geology* **17**, 534–537.
- Naar, D. F. & Hey, R. N. 1989b Recent Pacific–Easter–Nazca plate motions. *Evolution of mid-ocean ridges* (ed. J. M. Sinton). Geophysical monograph 57, pp. 9–30.
- Naar, D. F. & Hey, R. N. 1991 Tectonic evolution of the Easter microplate. *J. Geophys. Res.* **96**, 7961–7993.
- Naar, D. F., Martinez, F., Hey, R. N., Reed IV, T. B. & Stein, S. 1991 Pito rift: how a large offset rift propagates. *Mar. Geophys. Res.* **13**, 287–309.
- Nicolas, A., Freydier, C., Godard, M. & Vauchez, A. 1993 Magma chambers at oceanic ridges: how large? *Geology* **21**, 53–56.
- Nicolas, A., Boudier, F. & Ildefonse, B. 1994 Evidence from the Oman ophiolite for active mantle upwelling beneath a fast spreading ridge. *Nature* **370**, 51–53.
- Nicolas, A., Boudier, F. & Ildefonse, B. 1996 Variable crustal thickness in the Oman ophiolite: implication for oceanic crust. *J. Geophys. Res.* **101**, 17 941–17 950.
- Parmentier, E. M. & Phipps Morgan, J. 1990 Spreading rate dependence of three-dimensional structure in oceanic spreading centres. *Nature* **348**, 325–328.
- Perram, L. J., Cormier, M.-H. & Macdonald, K. C. 1993 Magnetic and tectonic studies of the dueling propagating spreading centres at 20° 40' S on the East Pacific Rise: evidence for crustal rotations. *J. Geophys. Res.* **98**, 13 835–13 850.

- Phipps Morgan, J. & Parmentier, E. M. 1985 Causes and rate-limiting mechanisms of ridge propagation: a fracture mechanics model. *J. Geophys. Res.* **90**, 8603–8612.
- Phipps Morgan, J. & Forsyth, D. W. 1988 Three dimensional flow and temperature perturbations due to a transform offset: effect on oceanic crustal and upper mantle structure. *J. Geophys. Res.* **93**, 2955–2966.
- Phipps Morgan, J. & Chen, Y. J. 1993 Dependence of ridge-axis morphology on magma supply and spreading rate. *Nature* **364**, 706–708.
- Phipps Morgan, J. & Sandwell, D. T. 1994 Systematics of ridge propagation south of 30° S. *Earth Planet. Sci. Lett.* **121**, 245–258.
- Phipps Morgan, J. & Parmentier, E. M. 1995 Crenulated seafloor: evidence for spreading-rate dependent structure of mantle upwelling and melting beneath a mid-ocean spreading centre. *Earth Planet. Sci. Lett.* **129**, 73–84.
- Rea, D. K. 1978 Asymmetric sea-floor spreading and a nontransform axis offset: the East Pacific Rise 20° S survey area. *Geol. Soc. Am. Bull.* **89**, 836–844.
- Rea, D. K. 1981 Tectonics of the Nazca–Pacific divergent plate boundary. *Nazca plate: crustal formation and Andean convergence* (ed. L. D. Kulm *et al.*), pp. 27–62. Geol. Soc. Am. Memoir no. 154.
- Renard, V., Hèkinian, R., Francheteau, J., Ballard, R. D. & Bäcker, H. 1985 Submersible observations at the axis of the ultra-fast-spreading East Pacific Rise (17° 30' to 21° 30' S). *Earth Planet. Sci. Lett.* **75**, 339–353.
- Rusby, R. I. & Searle, R. C. 1995 A history of the Easter microplate, 5.25 Ma to present. *J. Geophys. Res.* **100**, 12 617–12 640.
- Sandwell, D. T., Yale, M. M. & Smith, W. H. F. 1994 ERS-1 geodetic mission reveals detailed tectonic structures. *Eos* **75**, 155.
- Scheirer, D. S. & Macdonald, K. C. 1993 The variation in cross-sectional area of the axial ridge along the East Pacific Rise: evidence for the magmatic budget of a fast-spreading centre. *J. Geophys. Res.* **98**, 7871–7885.
- Scheirer, D. S., Macdonald, K. C., Forsyth, D. W., Miller, S. P., Wright, D. J., Cormier, M.-H. & Weiland, C. M. 1996a A map series of the southern East Pacific Rise and its flanks, 15° S to 19° S. *Mar. Geophys. Res.* **18**, 1–12.
- Scheirer, D. S., Macdonald, K. C., Forsyth, D. W. & Shen, Y. 1996b Abundant seamounts of the Rano Rahi seamount field near the southern East Pacific Rise, 15°–19° S. *Mar. Geophys. Res.* **18**, 13–52.
- Searle, R. C. 1983 Multiple, closely spaced transform faults in fast-slipping fracture zones. *Geology* **11**, 607–610.
- Searle, R. C. 1984 Gloria survey of the East Pacific Rise near 3.5° S: tectonic and volcanic characteristics of a fast spreading mid-ocean rise. *Tectonophysics* **101**, 319–344.
- Searle, R. C. & Francheteau, J. 1986 Morphology and tectonics of the Galapagos triple junction. *Mar. Geophys. Res.* **8**, 98–129.
- Searle, R. C., Rusby, R. I., Engeln, J., Hey, R. N., Zukin, J., Hunter, P. M., LeBas, T. P., Hoffman, H. J. & Livermore, R. 1989 Comprehensive sonar imaging of the Easter microplate. *Nature* **341**, 701–705.
- Sempère, J.-C., Macdonald, K. C., Miller, S. P. & Shure, L. 1987 Detailed study of the Brunhes/Matuyama reversal boundary on the East Pacific Rise at 19° 30' S: implication for crustal emplacement processes at an ultrafast spreading centre. *Mar. Geophys. Res.* **9**, 1–23.
- Shen, Y., Forsyth, D. W., Scheirer, D. S. & Macdonald, K. C. 1993 Two forms of volcanism: implications for the volume of off-axis crustal production on the west flank of the East Pacific Rise. *J. Geophys. Res.* **98**, 17 875–17 889.
- Shen, Y., Scheirer, D. S., Forsyth, D. W. & Macdonald, K. C. 1995 Trade-off in production between adjacent seamount chains near the East Pacific Rise. *Nature* **373**, 14–142.
- Sinton, J. M., Smaglik, S. M., Mahoney, J. J. & Macdonald, K. C. 1991 Magmatic processes at superfast mid-ocean ridges: glass compositional variations along the East-Pacific Rise 13°–23° S. *J. Geophys. Res.* **96**, 6133–6155.
- Sinton, J. M. & Detrick, R. S. 1992 Mid-ocean ridge magma chambers. *J. Geophys. Res.* **97**, 197–216.

- Sparks, D. W. & Parmentier, E. M. 1993 The structure of three-dimensional convection beneath oceanic spreading centres. *Geophys. J. Int.* **112**, 81–92.
- Tolstoy, M., Harding, A. J. & Orcutt, J. A. 1993 Crustal thickness on the Mid-Atlantic Ridge: bull's eye gravity anomalies and focused accretion. *Science* **262**, 726–728.
- Tolstoy, M., Harding, A. J., Orcutt, J. A. & the TERA Group 1997 Deepening of the axial magma chamber on the southern East Pacific Rise toward the Garrett fracture zone. *J. Geophys. Res.* (In the press.)
- Toomey, D. R., Purdy, G. M., Solomon, S. C. & Wilcock, W. S. D. 1990 The three-dimensional seismic velocity structure of the East Pacific Rise near latitude 9° 30' N. *Nature* **347**, 639–645.
- Tucholke, B. E. & Lin, J. 1994 A geological model for the structure of ridge segments in slow spreading ocean crust. *J. Geophys. Res.* **99**, 11 937–11 958.
- Tucholke, B. E. & Schouten, H. 1989 Kane fracture zone. *Mar. Geophys. Res.* **10**, 1–40.
- Urabe, T., Baker, E. T. & others 1995 The effect of magmatic activity on hydrothermal venting along the superfast-spreading East Pacific Rise. *Science* **269**, 1092–1095.
- Vera, E. E., Mutter, J. C., Buhl, P., Orcutt, J. A., Harding, A. J., Kappus, M. E., Detrick, R. S. & Brocher, T. M. 1990 The structure of 0 to 0.2 my old oceanic crust at 9° N on the East Pacific Rise from expanded spread profiles. *J. Geophys. Res.* **95**, 15 529–15 556.
- Wang, X. & Cochran, J. R. 1993 Gravity anomalies, isostasy, and mantle flow at the East Pacific Rise crest. *J. Geophys. Res.* **98**, 19 505–19 531.
- Wang, X., Cochran, J. R. & Barth, G. A. 1995 Gravity anomalies, crustal thicknesses and the pattern of mantle flow at the fast spreading East Pacific Rise, 9°–10° N: evidence for three-dimensional upwelling. *J. Geophys. Res.* **101**, 17 927–17 940.
- White, R. S., Detrick, R. S., Sinha, M. C. & Cormier, M.-H. 1984 Anomalous seismic crustal structure of oceanic fracture zones. *Geophys. Jl R. Astr. Soc.* **79**, 779–798.
- White, R. S., McKenzie, D. & O'Nions, R. K. 1992 Oceanic crustal thickness from seismic measurements and rare earth element inversions. *J. Geophys. Res.* **97**, 19 683–19 715.
- Wilson, D. S. 1992 Focused mantle upwelling beneath mid-ocean ridges: evidence from seamount formation and isostatic compensation of topography. *Earth Planet. Sci. Lett.* **113**, 41–55.
- Wilson, D. S., Hey, R. N. & Nishimura, C. 1984 Propagation as a mechanism of reorientation of the Juan de Fuca plate. *J. Geophys. Res.* **91**, 9215–9225.
- Wilson, D. S., Clague, D. A., Sleep, N. H. & Morton, J. L. 1988 Implications of magma convection for the size and temperature of magma chambers at fast spreading ridges. *J. Geophys. Res.* **93**, 11 974–11 984.